

Evidence for fast decay dynamics of the photoluminescence from Ge nanocrystals embedded in SiO₂

P.K. Giri^{a,*}, R. Kesavamoorthy^b, B.K. Panigrahi^b, K.G.M. Nair^b

^aDepartment of Physics, Indian Institute of Technology Guwahati, North Guwahati, Guwahati 781039, India

^bMaterials Science Division, Indira Gandhi Centre for Atomic Research, Kalpakkam 603102, India

Received 2 July 2004; accepted 3 November 2004 by J. Kuhl

Available online 11 November 2004

Abstract

We have investigated the origin of room temperature photoluminescence from ion-beam synthesized Ge nanocrystals (NCs) embedded in SiO₂ using steady state and time-resolved photoluminescence (PL) measurements. Ge NCs of diameter 4–13 nm were grown embedded in a thermally grown SiO₂ layer by Ge⁺ ion implantation and subsequent annealing. Steady state PL spectra show a peak at ~2.1 eV originating from Ge NCs and another peak at ~2.3 eV arising from ion-beam induced defects in the SiO₂ matrix. Time-resolved PL studies reveal double exponential decay dynamics on the nanoseconds time scale. The faster component of the decay with a time constant $\tau_1 \sim 3.1$ ns is attributed to the nonradiative lifetime, since the time constant reduces with increasing defect density. The slower component with time constant $\tau_2 \sim 10$ ns is attributed to radiative recombination at the Ge NCs. Our results are in close agreement with the theoretically predicted radiative lifetime for small Ge NCs.

© 2004 Elsevier Ltd. All rights reserved.

PACS: 78.47.+p; 78.67.Bf; 61.46.+w; 78.55.-m

Keywords: A. Germanium; A. Nanocrystals; D. Ion implantation; E. Photoluminescence

1. Introduction

Over the last decade, studies on the optical properties of group IV semiconductor nanocrystals (NCs) have drawn considerable attention owing to their potential application in Si-based optoelectronics [1] and electronic/optical memory devices [2]. Promising results have been achieved from Si NCs with optical gain [3] and tunable light emission [4] property. However, NC Si of several nanometers in diameter shows indirect band gap nature [5] and this results in a relatively long photoluminescence (PL) lifetime [6,7], which is one of the main obstacles to realizing Si-based

light emitting devices. In contrast, Ge NCs show a stronger confinement effect resulting in a direct gap semiconductor nature [8]. Consequently, there have been a lot of theoretical predictions on the superior optical properties of Ge NCs [9] as compared to the Si NCs. However, there exists substantial controversy about the origin of intense visible PL from Ge NCs [10,11], as several studies have indicated that the defects in the host matrix are primarily responsible for broad PL in the visible region [12,13]. Some experiments have indicated that a new structure of Ge different from that of the diamond structure exhibits the visible PL [14]. Size dependent near-infrared PL [15] and fast ($\ll 1$ μ s) PL decay dynamics [16] from Ge NCs have been attributed to quantum confinement effects, though theoretical studies predict the involvement of deep traps in the gap states of NC Ge as centers responsible for such emission [17]. Studies using several complementary techniques clearly demonstrated that infrared PL

* Corresponding author. Tel.: +91 361 258 2703; fax: +91 361 269 0762.

E-mail address: giri@iitg.ernet.in (P.K. Giri).

originates from defect states in the NCs [13]. A recent X-ray absorption spectroscopy study [18] provides conclusive evidence for stronger quantum confinement effects in the conduction band of Ge NCs as compared to similarly sized NC Si. However, its implications for the optoelectronic applications are not fully explored.

A powerful technique to explore dynamical characteristics of the carriers that contribute to the PL is time-resolved PL spectroscopy [19]. There have been several reports on time resolved PL spectroscopy of Si nanowires [20] and nanocrystals [21], which reveal anomalous dispersion relaxation of photoexcited carriers resulting in a stretched exponential decay of photoluminescence. Recent PL decay studies on Si NCs have shown that stretched exponential decay is an inherent property of individual Si NC [22]. Since, the exciton Bohr radius of bulk Ge crystal (17.7 nm) is much larger than that of bulk Si crystal (4.9 nm), the quantum size effects will appear more conspicuously for NC Ge than NC Si. However, properties those are sensitive to the size of the Ge NCs and properties that are sensitive to the environment and the macroscopic characteristics of the medium have not been distinguished properly. When the size of the NC is decreased the number of atoms located on its surface increases and optical properties will be greatly influenced by the surface condition. While theoretical studies predict several orders of magnitude lower lifetime in NC Ge (typically a few ns) as compared to NC Si (typically in the range μs – ms) [24], there is a lack of experimental evidence in support of the prediction. Niquet et al. [17] predicted that the radiative lifetime in NC Ge might be long (\sim few μs) in spite of the small difference (0.14 eV) between the direct and the indirect gap of bulk Ge. Reported results have indicated that the defects surrounding the NC Ge are responsible for the observed fast decay characteristics [16]. Hence, experimental determination of the radiative lifetime in NC Ge remains almost unexplored.

In this report, we study the steady state and transient decay characteristics of the photoluminescence from embedded Ge NC with varying NC size and surrounding defect density. From the steady state PL measurements, we first isolate the origin of various PL bands. Time resolved PL measurements show a considerably faster decay dynamics in NC Ge as compared to NC Si. These results are discussed in the context of theoretical predictions on the radiative lifetime of NC Ge.

2. Experimental details

For the present study, boron doped CZ grown Si (100) wafers were used as the substrates for growing SiO_2 layers of thickness \sim 300 nm by wet oxidation method. To synthesize the Ge NCs, 300 keV Ge^+ ion was implanted at room temperature on the SiO_2 layer with doses 3×10^{16} (Ge1), 1×10^{17} (Ge2) and 2×10^{17} (Ge3) ions/ cm^2 . SRIM

calculation, a Monte Carlo code, showed that the implanted Ge ions penetrate to a depth of \sim 350 nm and the peak of the ion distribution occurs at a depth of \sim 205 nm in SiO_2 layer. To study the growth of Ge NCs, implanted and unimplanted SiO_2 layers were heat-treated at 800 °C for 1 h and further treated at 950 °C for 2 h in argon gas ambient. Glancing incidence X-ray diffraction (XRD) and Raman scattering measurements were used to detect the formation of NC Ge in SiO_2 after each step of annealing. Samples were excited with 488 nm laser beam and the steady state PL emission spectra at room temperature (RT) were recorded using a double monochromator attached with a cooled photomultiplier tube and photon counting system. The PL decay measurements were performed at RT using 495 nm excitation pulse of 1.32 ns duration using a commercial fluorescence lifetime setup with a time resolution of 0.113 ns (Model IBH Fluorocube). In the decay measurement, a cutoff filter was placed before the emission detector to block the light below the wavelength 550 nm.

3. Results and discussion

The growth of Ge NCs in SiO_2 matrix was evaluated by XRD measurements in the glancing incidence mode using a powder diffractometer. Fig. 1 shows a set of XRD spectra recorded with an incidence angle of 3° on Ge2 sample post-annealed at 800 °C (curve 1) and 950 °C (curve 2). For comparison, spectrum from single crystalline Ge wafer (c-Ge) is also presented (curve 3) in Fig. 1. Curve 1 shows a

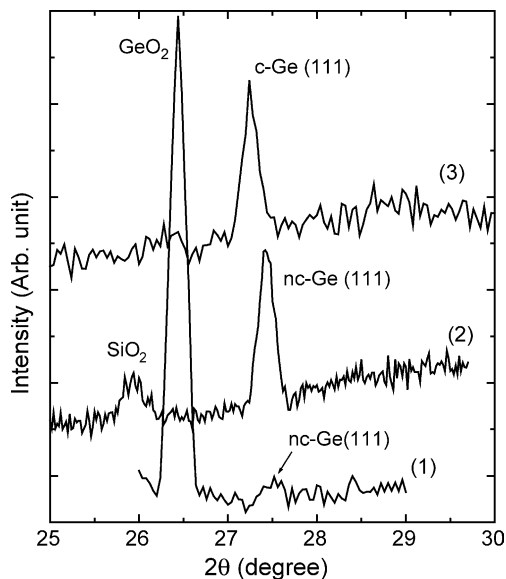


Fig. 1. Glancing incidence XRD spectra of ion-beam synthesized Ge NCs (nc-Ge) formed by post-annealing at (1) 800 °C for 1 h, (2) 950 °C for 2 h. For comparison, spectrum of single crystalline Ge wafer (c-Ge) is also shown (3). Different spectra are arbitrarily shifted along Y-axis for clarity of presentation.

strong Bragg peak at 26.44° and a weak peak at $\sim 27.4^\circ$, corresponding to GeO_2 and $\text{Ge}(111)$ NCs, respectively. 27.4° (2θ) peak is weak due to the very small size of the NCs and the residual ion damage in SiO_2 layer. After 950°C annealing, 27.4° (2θ) peak became strong due to larger volume fraction of $\text{Ge}(111)$ NCs. The small peak at 26.0° is attributed to the SiO_2 layer. Nanocrystalline $\text{Ge}(311)$ peak was also observed at 53.7° in 950°C annealed sample (not shown). Due to the inherent limitation of the XRD apparatus, observed peak width cannot be used as a measure of the particle size. To determine the size of the NCs, we recorded low frequency Raman spectra (LFRS) [25] on these samples. LFRS modes arise from the surface acoustic phonons of Ge NCs at the interface between the crystallite and the embedding dielectric matrix, and its frequency is inversely proportional to the size of the NCs [25]. LFRS of 800°C annealed samples show a peak at 21.2 cm^{-1} in Ge1 and 15.7 cm^{-1} in Ge2 sample. After 950°C annealing, these peaks shift to 13.8 and 6.5 cm^{-1} , respectively, indicating the NC size increase. The average diameter of the NCs estimated from LFRS varies from 4 to 13 nm depending on the ion dose and annealing temperature and shown in Table 1. Table 1 shows that Ge nanocluster grows with the increase in the ion dose as well as the annealing temperature. For a particular dose, NC size increased as the annealing temperature increased from 800 to 950°C . Note that NCs fabricated by ion implantation method usually show a wide distribution of size and the measured size is the average of the sizes present in the matrix. In the present study, NCs were biggest at 1×10^{17} ions/ cm^2 after 950°C post-annealing. Details of the LFRS spectra and analysis will be presented elsewhere [26].

Fig. 2 shows a set of PL spectra for 800°C annealed samples implanted with different doses. The 800°C annealed, unimplanted, wet oxidation grown SiO_2 layer on Si substrate shows a very weak PL band at $\sim 2.25\text{ eV}$ (not shown here) due to defects in the SiO_2 layer. This PL band intensity substantially reduces when further annealed at 950°C . This PL was subtracted from the PL spectra of 800°C annealed, implanted samples and shown in Fig. 2. The unconvoluted PL spectra show an intense and broad PL band at $\sim 2.19\text{ eV}$ for three different doses. After 950°C

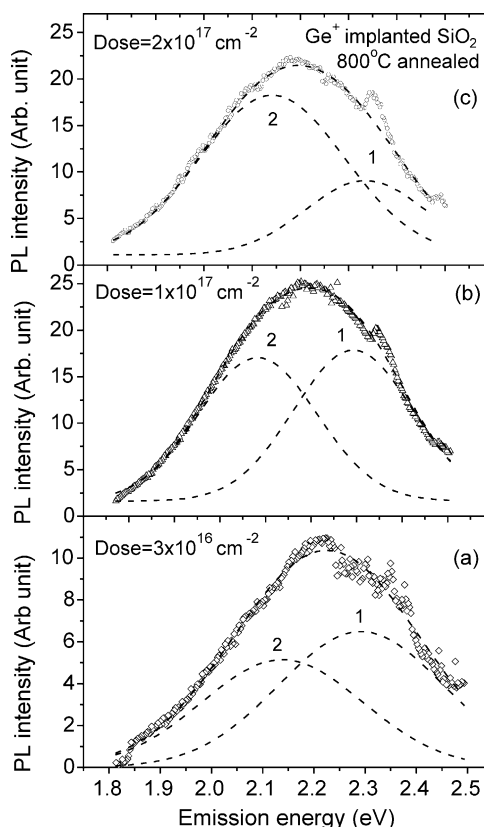


Fig. 2. Room temperature PL spectra (with symbols) of NC Ge prepared at 800°C for three different doses: (a) $3 \times 10^{16}\text{ cm}^{-2}$, (b) $1 \times 10^{17}\text{ cm}^{-2}$, (c) $2 \times 10^{17}\text{ cm}^{-2}$. Two Gaussian peaks are fitted (dashed lines) with the experimentally observed PL spectra. Fitting parameters are presented in Table 1.

annealing, the PL peak shifts to $\sim 2.32\text{ eV}$ as shown in Fig. 3. This apparent observed blue-shift of the PL on increasing the annealing temperature is inconsistent with the quantum confinement model of excitonic recombination in the NCs since LFRS results show an increase in NC Ge diameter (Table 1) which is expected to show a red-shift of PL peak. Hence, the major contribution to PL emission is unlikely to originate from Ge nanocrystals. A closer look at the

Table 1

Fitting parameters for the two Gaussian peaks (peak 1 and peak 2 shown in Figs. 2 and 3) fitted with the PL spectra observed for different samples. Mean size (diameter) of the NCs are determined from the LFRS peak position (see text)

Ge dose (cm^{-2})	800 °C Annealing					950 °C Annealing				
	Peak 1		Peak 2		NC size (nm)	Peak 1		Peak 2		NC size (nm)
	Center (eV)	FWHM (eV)	Center (eV)	FWHM (eV)		Center (eV)	FWHM (eV)	Center (eV)	FWHM (eV)	
3×10^{16}	2.29	0.32	2.14	0.31	4.0	2.32	0.35	2.03	0.21	6.1
1×10^{17}	2.29	0.26	2.08	0.26	5.4	2.33	0.32	2.06	0.23	13.0
2×10^{17}	2.33	0.25	2.14	0.30	4.1	2.30	0.33	2.03	0.22	9.2

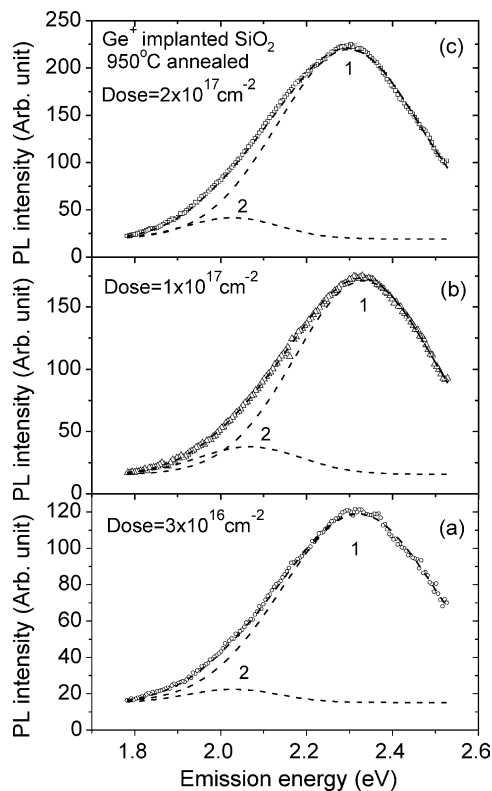


Fig. 3. Room temperature PL spectra (with symbols) of NC Ge prepared at 950 °C for three different doses: (a) $3 \times 10^{16} \text{ cm}^{-2}$, (b) $1 \times 10^{17} \text{ cm}^{-2}$, (c) $2 \times 10^{17} \text{ cm}^{-2}$. Two Gaussian peaks are fitted (dashed lines) with the experimentally observed PL spectra. Fitting parameters are shown in Table 1.

asymmetric line shape of the spectra in Figs. 2 and 3 reveals that the observed peak can be resolved into two Gaussian peaks. Fitting parameters thus obtained are shown in Table 1. The fitted data show that besides the major peak at $\sim 2.3 \text{ eV}$ (peak 1) that is common to 800 and 950 °C annealed samples, 800 °C annealed sample show a lower energy peak (peak 2) at $\sim 2.1 \text{ eV}$, and after 950 °C annealing this peak red-shifts to $\sim 2.0 \text{ eV}$ as expected from quantum confinement model. PL peak positions are almost independent of the ion dose, whereas relative peak intensity changes with dose. Annealed samples of 800 °C show comparable intensities for peak 1 and peak 2 (Fig. 2) while 950 °C annealed samples show that peak 1 is about 10 times more intense than peak 2.

From literature it is known that visible PL from Ge implanted SiO_2 layers primarily arise from a luminescent defect center [12]. Ge related P_b center has been found to be one major defect in Ge implanted SiO_2 layers. However, no unique energy has been associated with this defect emission band. Our unimplanted, 800 °C annealed SiO_2 layers on Si show a weak PL at 2.25 eV. All our implanted SiO_2 layers on Si show a PL component at $\sim 2.3 \text{ eV}$. This does not shift

with ion dose and annealing conditions. The intensity of this component increases with dose as seen from Figs. 2 and 3, except for 800 °C annealed 2×10^{17} dose sample. The defect density increases with dose and the PL intensity due to defects is expected to increase. Hence, this peak at 2.3 eV is attributed to defects. This PL intensity increases with annealing temperature, implying that the nonradiative recombination channels are reduced after annealing. A PL peak at $\sim 2.3 \text{ eV}$ has been reported by several groups from NC Ge [27], and has been argued to originate from defects at the Ge/ SiO_2 interface or in the SiO_2 matrix [12,13]. Si-implanted SiO_2 layers show similar PL spectra and it has been correlated with the oxygen deficient defects in SiO_2 as detected by paramagnetic resonance studies [28]. In the present study, these defects are created by Ge^+ -ion bombardment into SiO_2 and their density changes with dose and post-annealing temperature. It is known that Ge/GeO₂ interface related defects give rise to a PL peak at $\sim 3.1 \text{ eV}$ [29], which we cannot observe in our experiment with 2.54 eV excitation. Ion beam induced dangling bonds at the NC Ge/ SiO_2 interface has been identified as one major defect in such embedded system. Hence, the PL emission from these NCs is dominated by defects at the nanocrystal/ SiO_2 interface and surrounding SiO_2 matrix.

Data presented in Table 1 show that peak 2 is red-shifted by about 0.1 eV with the increase in the nanocrystal size from, say, 4.0 to 6.1 nm. This is fully consistent with the quantum confinement model of carrier recombination in NCs. Kim et al. [30] observed a PL peak at 2.1 eV from annealed Ge implanted SiO_2 , which was argued to originate from NC Ge. Maeda et al. [10] observed similar peak from NC Ge prepared by cosputtering method and argued in favor of the quantum confinement model for the observed peak. Hence, we attribute peak 2 at $\sim 2.1 \text{ eV}$ to the excitonic recombination at the NC Ge [12]. To verify the observed Ge NC related PL peak position with a simple quantum confinement (three dimensional) model of Brus [31], peak at $\sim 2.14 \text{ eV}$ would require a NC of 6.0 nm and 2.03 eV peak would require a NC of 6.3 nm. We have found similar size (4 nm for 2.14 eV peak and 6.1 nm for 2.03 eV peak) from low frequency Raman analysis (Table 1). However, experimentally determined size dependence of confinement energy is usually weaker than the theoretically predicted dependence, primarily due to the surface defects. Furthermore, due to the inherent size distribution in the ion-beam generated NCs broad PL band arises in the present case. Hence, exact calculation of the peak shifts cannot be done without the knowledge of the actual size distribution.

We performed time resolved PL measurements on the embedded Ge NCs to elucidate upon the dynamics of recombination. Fig. 4 shows the PL decay characteristics of samples implanted with different doses. As 2.3 eV PL band arises from the defects in the embedding matrix, to reduce the defect contribution to experimental decay data we use a 550 nm cutoff filter at the emission end. PL decay of similarly treated unimplanted SiO_2 layer was also recorded

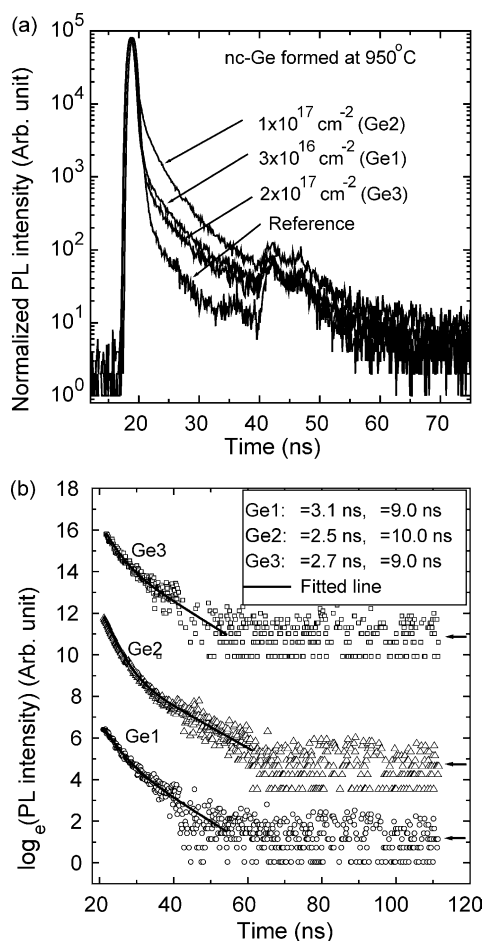


Fig. 4. (a) Room temperature PL decay characteristics (symbols) of the Ge NCs (nc-Ge) for samples Ge1, Ge2 and Ge3 annealed at 950 °C. System response is shown as ‘reference’ data. (b) Decay characteristics shown after subtracting the reference data from the sample spectra. The experimental data (symbols) are fitted with two exponential decay functions with time constants τ_1 and τ_2 and shown as solid line. The curves are arbitrarily shifted along Y-axis for clarity of presentation. In each case, amplitude of τ_1 dominates the decay behavior.

for comparison with implanted samples and they did not show any PL decay in the measured time scale (0.1–120 ns). Reference data shown in Fig. 4(a) refers to the system response for the lifetime measurement, which results from the scattering from a standard liquid sample. Reference data was subtracted from sample data to extract the decay time constant (τ). The observed decay characteristics shown over more than three orders of magnitude in intensity do not fit well with either a single exponential or a stretched exponential decay function. This in contrast to the PL decay observed for NC Si, which shows stretched exponential decay irrespective of the NC size and density. For the NC Ge, the experimental data could be fitted well with two exponential decay functions with time constants τ_1

and τ_2 for all ion doses. Fitting parameters thus obtained (Fig. 4(b)) show that τ_1 decreases from 3.1 to 2.5 ns with the increase in dose, while τ_2 does not change appreciably with dose. More interestingly, the amplitude of the fast decay component (τ_1) is very high compared to that of the slower decay component (τ_2) such that a major portion of the decay curve fits to a single exponential. Ratio of the amplitudes for the fast component and the slow component ranges from 233 to 6142, depending on the dose. This dose dependence of the τ_1 can be understood by considering the nonradiative recombination at the deep level defects. As the defect density increases with increasing ion dose, nonradiative recombination lifetime is expected to decrease with dose according to the Shockley-Read-Hall recombination theory [32]. Hence, the fast decay component can be attributed to the nonradiative recombination lifetime. In contrast, time constant τ_2 does not change with dose and seems to be a characteristic of the carrier recombination at the Ge NC bulk. This is consistent with the observation of a low intensity PL band at ~ 2.1 eV from steady state measurement. Note that in contrast to a very large PL lifetime (ranging from μ s to ms) reported for NC Si, NC Ge shows extremely fast (~ 10 ns) decay dynamics. Despite the presence of a large size distribution in the Ge NCs, exponential decay with a very fast dynamics is observed from our samples. This fast decay dynamics may be a consequence of the quantum confinement effect that results in increased oscillator strength of transition.

Weissker et al. [24] have predicted that in NC Ge the variation of lifetime with size would be less than one order of magnitude as compared to the lifetime variation (about five orders of magnitude) found in NC Si. The different radiative behavior of Si and Ge NCs is a consequence of the remarkable difference in their oscillator strengths [24]. Takeoka et al. [16] reported the lifetime of NC Ge to be shorter than 40 ns for the near-infrared PL emission from very small NC Ge, whereas Aoki et al. [33] did not find a nanosecond PL lifetime component. In the literature, near-infrared PL emission from NC Ge has been ascribed to interfacial oxygen deficient type defects between the oxide and the NC Ge [13]. Depending on the method of calculations, theoretically predicted lifetime varies typically from ~ 10 ns [24] to ~ 100 μ s [17] for small NC Ge. As the direct band gap of Ge is very close to the indirect gap of Ge crystals, the PL lifetime for band to band transition in Ge is expected to be quite small as compared to that of Si. In NC Ge, this transition probability is further enhanced due to the relaxation of k-conservation rule [5]. Hence, observed fast decay dynamics may be justified. Our results are in close agreement with the theoretically predicted radiative lifetime of ~ 10 ns for NC Ge [24]. Hence, the observed τ_2 (~ 9 – 10 ns) is a characteristic of the NC Ge, while τ_1 (2.5–3.1 ns) is the nonradiative recombination time associated with the defects. The nonradiative relaxation procedure might take place at surface dangling bonds of NC Ge or the interface between NC Ge and SiO₂ matrix. The presence of dangling

bonds at the NC Ge surface affects the radiative efficiency and controls the overall luminescence efficiency. It should be noted that observed PL efficiency of NC Ge is much lower than predicted theoretically, and this is attributed to the large amount of defects present in the surrounding matrix that acts as nonradiative recombination channels. Studies on NCs prepared by other methods with controlled defects would be required to explore the expected high quantum efficiency.

4. Conclusions

In conclusion, we provide experimental evidence of a fast radiative recombination in Ge NCs. From the steady state PL measurements, we show that the ~ 2.3 eV PL emission from ion-beam synthesized NCs is primarily contributed by the defects in the SiO₂ matrix, whereas the ~ 2.1 eV PL band is attributed to radiative recombination at the Ge NCs. Time-resolved measurements reveal that the fast component ($\tau = 2.5\text{--}3.0$ ns) of the decay is the nonradiative lifetime of carriers, while the slower component ($\tau = 9\text{--}10$ ns) is attributed to the radiative recombination lifetime of carriers at the Ge NCs.

Acknowledgements

We gratefully acknowledge the help provided by S. Sarma, A. Srinivasan, L. Homachaudhury, P. Magudapathy, S. Dhara, B. Sundaravel, S. Amirtapandian, and David in performing various experiments related to this work.

References

- [1] H. Zimmermann, *Integrated Silicon Opto-electronics*, Springer, Berlin, 2000; L. Pavesi, S. Gaponenko, L. Dal Negro, *Towards the First Silicon Laser*, Kluwer Academic Publishers, Dordrecht, 2003.
- [2] W.K. Choi, W.K. China, C.L. Heng, L.W. Teo, V. Ho, V. Ng, D.A. Antoniadis, E.A. Fitzgerald, *Appl. Phys. Lett.* 80 (2002) 2014.
- [3] L. Pavesi, L. Dal Negro, C. Mazzoleni, G. Franzo, F. Priolo, *Nature (London)* 408 (2000) 440.
- [4] G. Ledoux, J. Gong, F. Huisken, O. Guillous, C. Reynaud, *Appl. Phys. Lett.* 80 (2002) 4834.
- [5] D. Kovalev, H. Heckler, M. Ben-Chorin, G. Polisski, M. Schwartzkopff, F. Koch, *Phys. Rev. Lett.* 81 (1998) 2803.
- [6] S. Takeoka, M. Fujii, H. Hayashi, *Phys. Rev. B* 62 (2000) 16820.
- [7] C. Garcia, B. Garrido, P. Pellegrino, R. Ferre, J.A. Moreno, J.R. Morante, L. Pavesi, M. Cazzanelli, *Appl. Phys. Lett.* 82 (2003) 1595.
- [8] J.R. Heath, J.J. Shiang, A.P. Alivisatos, *J. Chem. Phys.* 101 (1994) 1607.
- [9] H.-Ch. Weissker, J. Furthmüller, F. Bechstedt, *Phys. Rev. B* 65 (2002) 155327; H.-Ch. Weissker, J. Furthmüller, F. Bechstedt, *Phys. Rev. B* 65 (2002) 155328.
- [10] Y. Maeda, *Phys. Rev. B* 51 (1995) 1658.
- [11] J. Zhang, X. Bao, Y. Ye, X. Tan, *Appl. Phys. Lett.* 73 (1998) 1790.
- [12] K.S. Min, K.V. Shcheglov, C.M. Yang, H.A. Atwater, M.L. Brongersma, A. Polman, *Appl. Phys. Lett.* 68 (1996) 2511.
- [13] X.L. Wu, T. Gao, G.G. Siu, S. Tong, X.M. Bao, *Appl. Phys. Lett.* 74 (1999) 2420.
- [14] Y. Kanimetsu, H. Uto, Y. Masumoto, Y. Maeda, *Appl. Phys. Lett.* 61 (1992) 2187.
- [15] S. Takeoka, M. Fujii, S. Hayashi, K. Yamamoto, *Phys. Rev. B* 58 (1998) 7921.
- [16] S. Takeoka, M. Fujii, S. Hayashi, K. Yamamoto, *Appl. Phys. Lett.* 74 (1999) 1558.
- [17] Y.M. Niquet, G. Allan, C. Dellerue, M. Lanoo, *Appl. Phys. Lett.* 77 (2000) 1182.
- [18] C. Bostedt, T. Van Burren, T.M. Willey, N. Franco, L.J. Terminello, C. Heske, T. Moller, *Appl. Phys. Lett.* 84 (2004) 4056.
- [19] H. Stolz, *Time-resolved Scattering from Excitons*, Springer, Berlin, 1994.
- [20] L. Pavesi, M. Ceschini, *Phys. Rev. B* 48 (1993) 17625.
- [21] M. Dovrat, Y. Goshen, J. Jedrzejewski, I. Balberg, A. Sa'ar, *Phys. Rev. B* 69 (2004) 155311.
- [22] O. Guillois, N. Herlin-Boime, C. Reynaud, G. Ledoux, F. Huisken, *J. Appl. Phys.* 95 (2004) 3677.
- [24] H.-Ch. Weissker, J. Furthmüller, F. Bechstedt, *Phys. Rev. B* 69 (2004) 115310; H.-Ch. Weissker, J. Furthmüller, F. Bechstedt, *Phys. Rev. B* 67 (2003) 245304.
- [25] E. Duval, A. Boukenter, B. Champagnon, *Phys. Rev. Lett.* 56 (1986) 2052; S. Dhara, R. Kesavamoorthy, P. Magudapathy, M. Premila, B.K. Panigrahi, K.G.M. Nair, C.T. Wu, K.H. Chen, L.C. Chen, *Chem. Phys. Lett.* 370 (2003) 254–260.
- [26] P.K. Giri, R. Kesavamoorthy, B.K. Panigrahi, K.G.M. Nair, unpublished.
- [27] See, for example S. Okamoto, Y. Kanimetsu, *Phys. Rev. B* 54 (1986) 16421.
- [28] V.Ya. Bratus, M.Ya. Valakh, I.P. Vorona, T.T. Petrenko, A.V. Yukhimchuk, P.L.F. Hemment, T. Komoda, *J. Lumin.* 80 (1999) 269.
- [29] M. Zacharias, P.M. Fauchet, *Appl. Phys. Lett.* 71 (1997) 380.
- [30] H.B. Kim, K.H. Chae, C.N. Whang, J.Y. Jeong, M.S. Oh, S. Im, J.H. Song, *J. Lumin.* 80 (1999) 281.
- [31] L.E. Brus, *IEEE J. Quantum Electron.* 22 (1986) 1909.
- [32] J. Singh, *Optoelectronics: An Introduction to Materials and Devices*, McGraw-Hill, New York, 1996 (chapter 5).
- [33] T. Aoki, S. Komeodoori, C. Fujiihashi, A. Ganjoo, K. Shimakawa, *J. Non-Cryst. Solids* 299–302 (2002) 642.